Title

Uptake of tumor-derived microparticles induces metabolic reprogramming of macrophages in the early metastatic lung

Authors

Kersten, Kelly

You, Ran

Liang, Sophia

et al.

Peer reviewed

Uptake of tumor-derived microparticles induces metabolic reprogramming of macrophages in the early metastatic lung

Kelly Kersten[1,2,7], **Ran You**[1,2,7], **Sophia Liang**[3], **Kevin M. Tharp**[4], **Joshua Pollack**[2,5], **Valerie M. Weaver**[4], **Matthew F. Krummel**[1,2,5], **Mark B. Headley**[3,6,8,*]

[1]Department of Pathology, University of California San Francisco, San Francisco, CA 94143, USA

[2]ImmunoX Initiative, University of California San Francisco, San Francisco, CA 94143, USA

[3]Clinical Research Division, Fred Hutchinson Cancer Research Center, Seattle, WA 98109, USA

[4]Center for Bioengineering and Tissue Regeneration, Department of Surgery, University of California San Francisco, San Francisco, CA 94143, USA

[5]Foundery Innovations, San Francisco, CA 94080, USA

[6]Department of Immunology, University of Washington, Seattle, WA 98109, USA

[7]These authors contributed equally

[8]Lead contact

SUMMARY

Pre-metastatic niche formation is a critical step during the metastatic spread of cancer. One way by which primary tumors prime host cells at future metastatic sites is through the shedding of tumor-derived microparticles as a consequence of vascular sheer flow. However, it remains unclear how the uptake of such particles by resident immune cells affects their phenotype and function. Here, we show that ingestion of tumor-derived microparticles by macrophages induces a rapid metabolic and phenotypic switch that is characterized by enhanced mitochondrial mass and function, increased oxidative phosphorylation, and upregulation of adhesion molecules, resulting in reduced motility in the early metastatic lung. This reprogramming event is dependent on signaling through the mTORC1, but not the mTORC2, pathway and is induced by uptake of tumor-derived microparticles. Together, these data support a mechanism by which uptake of

tumor-derived microparticles induces reprogramming of macrophages to shape their fate and function in the early metastatic lung.

Graphical abstract
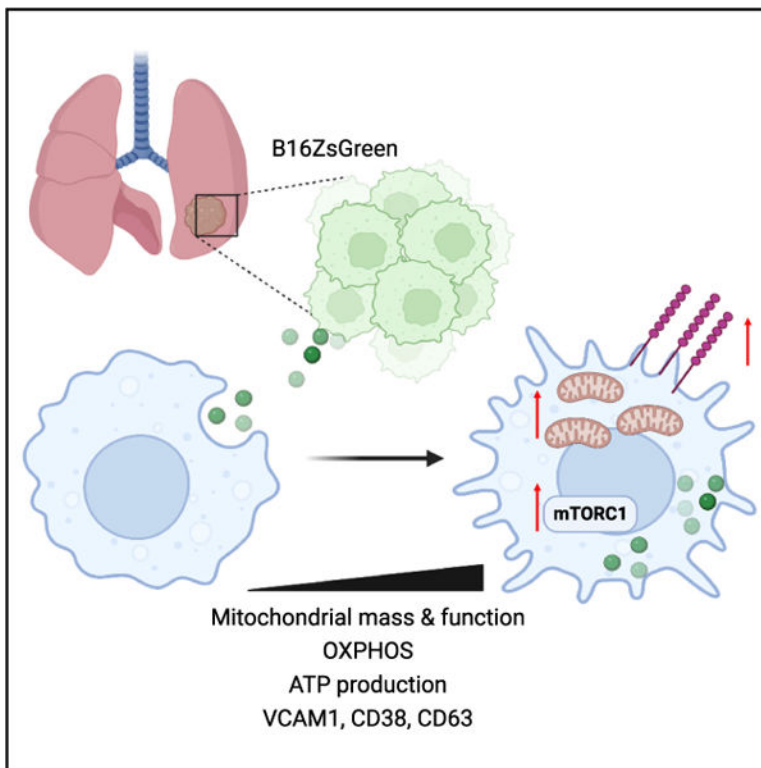
In brief

Kersten et al. show that ingestion of tumor-derived microparticles induces a metabolic and phenotypic switch in non-alveolar inflammatory macrophages in the early metastatic lung. This mTORC1-dependent reprogramming event, characterized by increased OXPHOS, ATP production, and upregulation of adhesion molecules, dictates macrophage phenotype and function during metastasis.

INTRODUCTION

Metastatic spread is one of the main causes of cancer mortality. Yet, the mechanisms by which cancer cells disseminate from the primary tumor and successfully colonize distant organs remains largely unknown. Accumulating evidence demonstrates a pivotal role for immune cells in priming distant organs by creating a ''pre-metastatic niche'' that supports the colonization and outgrowth of future incoming cancer cells. This is partly mediated by classical inflammatory monocytes and macrophages promoting metastatic spread of cancer through their regulation of tissue remodeling, angiogenesis, and suppressing anti-tumor T cell responses.[1–3] Conversely, a population of non-classical patrolling monocytes prevented the formation of lung metastasis by engulfing tumor-derived material and promoting natural

killer (NK) cell recruitment and activation.[4] The mechanisms by which tumor-derived factors instruct myeloid cells at these distant (pre)metastatic sites remain undiscovered.

Monocytes and macrophages display a remarkable heterogeneity and plasticity that is highly dependent on spatial and temporal cues from their local microenvironment. Several studies have reported the shedding of microparticles, including exosomes, as a way for tumors to instruct resident cells, including endothelial cells, fibroblasts, and macrophages, at distant organs to create a niche that is then susceptible to disseminated cancer cells and supports metastatic growth.[5–8] We have previously reported that primary B16F10 mouse melanomas shed microparticles that are rapidly ingested by distinct waves of myeloid populations in the early metastatic lung.[2] The majority of these microparticles, which we termed ''cytoplasts,'' had a diameter significantly larger (>1 μm) than that of tumor-derived exosomes (<200 nm) and exhibited autonomous motility.[2] Unlike ''karyoplasts,'' cytoplasts did not contain tumor-derived nuclei but did contain mitochondria, consistent with metabolic potential and motility. More recent work has referred to these tumor-derived particles as ''large extracellular vesicles'' or ''oncosomes.''[9] We demonstrated that non-alveolar inflammatory macrophages were the most predominant myeloid population ingesting these microparticles in the early metastatic lung.[2]

Here, we examined the early consequences of ingestion of tumor-derived material by macrophages, looking at their transcriptional profiles and changes in cellular metabolism to understand the nature of reprogramming of the myeloid compartment by early metastatic pioneers in the lung.

RESULTS

Ingestion of tumor-derived microparticles induces transcriptional reprogramming of macrophages in the early metastatic lung

To study the dynamics of antigen loading and how it affects the fate of myeloid populations in the early metastatic lung, we utilized an animal model for experimental metastasis by intravenous (i.v.) administration of a range of established cancer cell lines tagged with fluorescent marker ZsGreen (Figures 1A and 1B). In line with previous results,[2] we found a diverse range of ZsGreen antigen loading among distinct myeloid populations in the lung 24 h post i.v. injection of cancer cells (Figures 1B, S1A, and S1B). Among them, non-alveolar inflammatory macrophages were the most predominant cell type ingesting ZsGreen+ microparticles, accounting for ~50% of all ZsGreen+ CD45+ immune cells at 24 h post-exposure (Figures 1B and S1B). ZsGreen+ CD45+ cells displayed a lower mean fluorescence intensity compared with the injected B16ZsGreen cells (Figure S1B), suggesting that most of ingested tumor-derived material consisted of smaller microparticles compared with phagocytosed intact tumor cells. This loading occurred similarly following injection of ZsGreen-tagged Lewis lung carcinoma (LLC), the poorly metastatic B16F1, as well as non-cancerous ZsGreen-tagged mouse embryonic fibroblasts (MEFs) derived from β-actin[Cre];Ai6 mice (Figure 1B). In contrast, following i.v. administration of fluorescent latex beads, patrolling monocytes represented the majority of bead-ingesting immune cells (Figure 1B).

We next sought to ascertain whether gene and cell surface protein expression are modulated following ingestion of tumor-derived microparticles. We administered B16F10 cells tagged with ZsGreen (B16ZsGreen cells) i.v. and, 24 h later, performed cell surface proteomics on whole lung using our recently developed Infinity Flow method.[10] We comprehensively examined the cell surface proteome of the subset of tumor-ingesting versus non-ingesting macrophages in direct comparison with other lung myeloid subsets (Figures 1C and S1C) The tumor-ingesting macrophage population was identified based on high ZsGreen mean fluorescence intensity (MFI) (Figure S1D). This analysis revealed distinct phenotypic differences between macrophages and other lung myeloid cells and further revealed an array of cell surface markers that differed in expression between ZsGreen+ and ZsGreen− macrophages (Figure 1C). We additionally utilized fluorescence-activated cell sorting (FACS) to isolate lung macrophages that had ingested tumor-derived microparticles (ZsGreen+) versus those that had not (ZsGreen−) and performed RNA sequencing to assess differential gene expression between the two macrophage populations. Analysis of differentially expressed genes (DEGs) revealed that uptake of microparticles induced a rapid transcriptional reprogramming characterized by the upregulation of a range of mitochondrial genes (referred to as a ''mitochondrial signature'') as well as cellular adhesion markers (''surface signature''; e.g., *Vcam1*, *Cd38*, *Cd63*) (Figure 1D). Importantly, this cell surface signature aligned with that revealed by Infinity Flow (Figure 1E). Moreover, we found that expression of stimulatory dendritic cell (DC) genes–including *Flt3*, *Zbtb46*, *Ccr7*, and *Btla*–was significantly downregulated in ZsGreen+ versus ZsGreen− macrophages (''DC signature'') (Figure 1D), suggesting that this reprogramming event is phenotypically distinct from DC activation, which is often correlated with improved anti-tumor responses.[11,12] Together, these data demonstrate that macrophages loaded with tumor-derived microparticles display distinct transcriptional and phenotypic programs compared with non-loaded macrophages in the early metastatic lung.

Phenotypic reprogramming of lung macrophages upon antigen loading with tumor-derived microparticles

Based on the high concordance between protein and transcript levels, we selected cell surface markers CD63, VCAM1, and CD38 as a signature for further interrogation of the impact of tumor ingestion on lung macrophage populations using multiparameter flow cytometry (Figure 1E). We first validated the expression differences in independent flow cytometry experiments and confirmed the upregulation of VCAM1, CD38, and CD63 after ingestion of tumor-derived material on the surface of macrophages in the early metastatic lung but not on patrolling monocytes (Figures S2A and S2B). Importantly, *in-vitro*-cultured bone marrow-derived macrophages (BMDMs) similarly upregulated VCAM1, CD38, and CD63 on their surface in response to B16ZsGreen ingestion (Figures S2C and S2D), supporting the use of these proteins as a signature of ingestion-mediated modulation of macrophages. Antigen loading (Figure S3A) and the resulting phenotypic change in lung macrophages after B16ZsGreen injection occurred similarly after administration of MEFZsGreen cells *in vivo*, albeit less pronounced (Figures 2A and 2B). While VCAM1 and CD63 surface levels were only found augmented at 24 h injection, CD38 expression levels were already substantially upregulated 2 h after exposure (Figure S3C). Uptake of fluorescein isothiocyanate (FITC)-labeled beads modestly increased the expression of

VCAM1 and CD63 on lung macrophages, but the levels were significantly lower following ingestion of B16-derived microparticles (Figures S4A–S4H).

To assess whether the upregulation of adhesion molecules in ZsGreen$^+$ versus ZsGreen$^-$ macrophages affected macrophage patrolling behavior in the lung, we performed two-photon imaging in live lung slices obtained from MacBlue mice–in which ECFP expression is driven by a modified *c-Fms* promoter, allowing the visualization of monocytes, monocyte-derived macrophages, and a small proportion of neutrophils.[13] 24 h after i.v. injection of B16ZsGreen cells (Figure 2C), ZsGreen$^+$ ECFP$^+$ cells exhibited substantially lower motility compared with ZsGreen$^-$ ECFP$^+$ cells in the lung (Figures 2D and 2E). This slowing of macrophage patrolling behavior might be due to reduced cellintrinsic motility, a change of location relative to tissue, or the upregulation of expression of adhesion markers after uptake of microparticles.

Tumor-derived antigen loading drives mitochondrial reprogramming in lung macrophages

To further study macrophage phenotypic reprogramming in the early metastatic lung, we performed gene set enrichment analysis (GSEA) on our RNA sequencing (RNA-seq) dataset (Figure 1D). This revealed four major pathway networks closely associated with translation, protein processing, catabolic processes, and mitochondrial respiration that were highly enriched in ZsGreen$^+$ macrophages compared with ZsGreen$^-$ macrophages (Figure 3A; Table S1).

Following up on the ''mitochondrial signature'' induced in antigen-loaded macrophages (Figure 1D), we quantified the variation in mitochondrial mass (indicated by MitoTracker DeepRed staining) and mitochondrial membrane potential (DJm; determined by fluorescence of the potential-sensitive tetramethylrhodamine methyl [TMRM] dye) after *in vivo* antigen loading upon i.v. injection with B16ZsGreen or MEFZsGreen cells (Figure 3B). ZsGreen$^+$ macrophages exhibited a significant increase in mitochondrial mass, DJm, and TMRM^{hi}/TMRM^{low} ratio when compared with ZsGreen$^-$ macrophages from the same mice, consistent with our GSEA (Figures 3C and 3D). Notably, this was not the case for macrophages loaded with MEF-derived microparticles or FITC-labeled beads (Figures 3D and 3E), suggesting that the mitochondrial reprogramming of lung macrophages is induced exclusively upon antigen loading with tumor-derived material.

To extend this analysis to oxygen consumption rate (OCR), we developed an *in vitro* surrogate assay in which BMDMs are cultured with B16ZsGreen tumor cells and ZsGreen$^+$ and ZsGreen$^-$ BMDMs are isolated for study after 24 h (Figure 4A). Consistent with the increased mitochondrial density and membrane potential observed in macrophages directly *ex vivo* (Figures 3C–3E), ZsGreen$^+$ BMDMs from this *in vitro* exposure showed a significantly higher OCR with higher basal and maximal respiration, as well as increased ATP production, when compared with ZsGreen$^-$ BMDMs or non-tumor (NT) BMDMs, which had never encountered tumor cells (Figures 4B and 4C). Moreover, the spare respiratory capacity (SRC) was increased in ZsGreen$^+$ BMDMs, suggesting an improved capability to respond to sudden changes in energy demand (Figure 4C). To determine whether this was phenocopied in cells that were programmed through exposure *in vivo*, we isolated lung macrophages from B16ZsGreen-challenged mice and compared their OCRs

with lung macrophages from unchallenged (NT) mice. In line with our *in vitro* data, lung macrophages that encountered tumor material showed increased OCRs compared with NT mice (Figure S5A and S5B). To test whether this metabolic shift in lung macrophages is dictated by the source of antigen, we sorted ZsGreen$^+$ and ZsGreen$^-$ macrophages from the lungs of either B16ZsGreen- or MEFZsGreen-injected mice (Figure 4D) and determined their ATP production as a direct measurement of mitochondrial function. While antigen loading of macrophages with B16-derived microparticles induced a significant increase in ATP production in ZsGreen$^+$ versus ZsGreen$^-$ macrophages, loading with MEF-derived microparticles did not (Figure 4E). Taken together, our data show that antigen loading with tumor-derived material specifically enhanced mitochondrial respiration and increased ATP production in lung macrophages.

Macrophage reprogramming upon ingestion of tumor-derived microparticles is mTORC dependent

To study the pathways regulating reprogramming of lung macrophages after ingestion of tumor-derived microparticles, we performed hallmark pathway analysis comparing the transcriptional profiles of ZsGreen$^-$ and ZsGreen$^+$ macrophages. We identified several metabolism-associated pathways, among which ''oxidative phosphorylation'' was highly enriched in ZsGreen$^+$ versus ZsGreen$^-$ macrophages (Figure 5A, indicated with green dot). The mammalian target of rapamycin (mTOR)–the catalytic sub-unit of the two distinct complexes mTORC1 and mTORC2–is a central regulator of cellular metabolism and has been shown to drive mitochondrial biogenesis and oxidative function.[14,15] Macrophage activation is dependent on mTOR, and roles for both mTORC1[16] and mTORC2[17,18] have been implicated. Although it did not reach statistical significance in our dataset, mTORC1 signaling was among the enriched pathways in ZsGreen$^+$ versus ZsGreen$^-$ macrophages (Figure 5A, indicated with green dot). In line with this, detailed analysis of the genes that constitute the mTORC1 pathway revealed upregulation of genes encoding phospholipases D1 and 3 (*Pld1* and *Pld3*) and protein synthesis genes *Eif4ebp1*, *Rps23*, and *Ptpa* (Figure 5B). In contrast, expression of a positive regulator gene of AMP-activated protein kinase (AMPK), *Prkab2*, was downregulated in ZsGreen$^+$ versus ZsGreen$^-$ macrophages (Figure 5B), indicating that the AMPK pathway, as a negative upstream regulator of mTOR signaling,[19] was repressed. In line with our transcriptional data, we detected significantly higher levels of phosphorylated (p)4EBP1 and pS6 protein in ZsGreen$^+$ versus ZsGreen$^-$ macrophages by flow cytometry, confirming the activation of mTORC1 signaling upon ingestion of tumor-derived microparticles (Figure 5C).

To study whether the phenotypic switch in lung macrophages in response to ingestion of tumor-derived microparticles is regulated by mTOR, we treated mice intranasally with rapamycin to inhibit mTOR activation locally in the lungs of B16ZsGreen-injected mice. We found that upregulation of VCAM1, CD38, and CD63 expression on ZsGreen$^+$ lung macrophages was significantly abolished upon rapamycin treatment compared with DMSO-treated mice (Figure 5D). Through imaging, we also found that ZsGreen$^+$ myeloid cells in rapamycin-treated mice failed to arrest on lung parenchyma, in contrast to DMSO-treated controls (Figure 5E), suggesting that macrophage phenotypic reprogramming upon the ingestion of tumor-derived microparticles is dependent on mTORC signaling.

mTORC1 is required for metabolic and phenotypic reprogramming of macrophages in the early metastatic lung

Because intranasal administration of rapamycin does not exclusively target macrophages, we undertook a genetic approach to test the various contributions of the two mTORC signaling complexes; genetic loss of regulatory-associated protein of mTOR (Raptor) results in loss of the mTORC1 protein complex, while the mTORC2 complex is lost in mice lacking rapamycin-insensitive companion of mTOR (Rictor).[19] Using mice bearing conditional alleles *Raptor^f/f* and *Rictor^f/f* together with a Cre recombinase under the control of the lysozyme 2 gene, we generated mice with myeloid-specific deletion of mTORC1 (*Rptr^f/f LysM^Cre*) and mTORC2 (*Rctr^f/f LysM^Cre*) complexes, respectively (Figure 6A). These mice were bred to the C57BL/6J background for >10 generations to prevent any bias caused by mixed genetic backgrounds. While deficiency of mTORC1 or mTORC2 did not affect the proportion of lung macrophages, nor their ability to ingest ZsGreen⁺ tumor-derived microparticles (Figure S6A and S6B), we detected a significant reduction in the ability to increase mitochondrial mass, membrane potential, and mitochondrial function in ZsGreen⁺ versus ZsGreen⁻ macrophages in *Rptr^f/f LysM^Cre* mice compared with wild-type (WT) littermates or *Rctr^f/f LysM^Cre* mice (Figure 6B), demonstrating that mTORC1 signaling, specifically, is required for the metabolic switch in macrophages upon antigen loading.

To directly test how mitochondrial metabolism in macrophages was affected after uptake of tumor-derived microparticles, we sorted ZsGreen⁺ and ZsGreen⁻ BMDMs after 24 h of co-culture with B16ZsGreen cells and monitored their metabolism of isotopically labeled glucose (^{13}C) for 2 h[20] (Figures 6C and S6C). Ingestion of ZsGreen⁺ microparticles by WT BMDMs (WT ZsGreen⁺ versus WT ZsGreen⁻) increased mitochondrial metabolism of glucose indicated by increased incorporation of ^{13}C into TCA cycle intermediates (Figure S6C), which corroborates our cellular respirometry data obtained with our Seahorse assays (Figures 4B, 4C, S5A, and S5B). This process was attenuated in mTORC1-deficient BMDMs derived from *Rptr^f/f LysM^Cre* mice (Figure S6C). Specifically, we found reduced isotopic labeling of succinate, malate, citrate, and alpha-ketoglutarate in ZsGreen⁺ *Rptr^f/f LysM^Cre* BMDMs compared with ZsGreen⁺ WT BMDMs (Figure 6D).

To validate our findings from the isotopic tracing experiment *in vivo*, we sorted ZsGreen⁺ and ZsGreen⁻ lung macrophages from WT, *Rptr^f/f LysM^Cre*, and *Rctr^f/f LysM^Cre* mice 24 h after i.v. injection of B16ZsGreen cells (Figure 6A) and directly measured their ATP production. Consistently, the increased ATP production in ZsGreen⁺ versus ZsGreen⁻ macrophages as observed in WT mice was completely abolished in *Rptr^f/f LysM^Cre* mice, while the absence of mTORC2 in macrophages from *Rctr^f/f LysM^Cre* mice displayed ATP production similar to controls (Figure 6E). Of note, while ZsGreen⁻ macrophages from *Rptr^f/f LysM^Cre* mice intrinsically showed a lower mitochondrial mass (Figure 5B) and isotopic labeling of succinate and alpha-ketoglutarate (Figure 5D), this did not result in a deficiency to produce ATP compared with *Rctr^f/f LysM^Cre* mice or WT littermates (Figure 5E). Moreover, upregulation of VCAM1 and CD63, but not CD38, on ZsGreen⁺ macrophages was significantly lower in *Rptr^f/f LysM^Cre* mice when compared with WT and *Rctr^f/f LysM^Cre* mice (Figure 6F). We thus conclude that metabolic and phenotypic

reprogramming of lung macrophages after uptake of tumor material is dependent on mTORC1 signaling.

Finally, to test the functional significance of mTORC1-dependent macrophage reprogramming for the clinical outcome of metastatic disease, we i.v. injected *Rptr^f/f LysM^Cre* mice and WT littermates with B16ZsGreen and allowed lung metastasis to develop. Interestingly, at 24 h post-i.v. injection with B16ZsGreen, we found a modest but significant increase in the proportion of ZsGreen⁺ CD45⁻ cells in the lungs of *Rptr^f/f LysM^Cre* mice compared with WT littermates (Figure 6F), suggestive of increased metastatic seeding. However, by 2–3 weeks of lung colonization, the total number of metastatic nodules (Figure S6D) or the metastatic burden (measured as the area of the lung affected by metastasis) (Figure S6E) was not affected by macrophage-specific mTORC1 deficiency. This normalization may be a result of local changes in nutrient availability as a result of rapidly growing tumor lesions dominating the lung metastatic microenvironment.

DISCUSSION

A number of studies have implicated the important role of macrophages in the metastatic spread of cancer.[21,22] However, it remains unclear how the early interactions between disseminated cancer cells and macrophages in pre-metastatic tissues dictate successful colonization of secondary organs. Previously, we and others have shown that tumors actively shed microparticles (including exosomes) into the circulation that migrate to and condition pre-metastatic sites such as the lungs.[2,6–8,23] Shedding of extracellular particles and vesicles has been observed in several physiological and pathological conditions.[9] Some studies have reported that these vesicles, released in conditions of cellular energetic stress, contain mitochondria or mitochondria-derived components.[2,5,24] However, how ingestion of these particles dictates immune cell phenotype and function in the context of the metastatic spread of cancer remains largely unknown. In this work, we have demonstrated that ingestion of tumor-derived microparticles induces a metabolic and phenotypic switch in non-resident macrophages in the early metastatic lung that is highly dependent on mTORC1 signaling. We found that this reprogramming event is specific for the uptake of tumor-derived material. Thus, these initial changes might be an important step for shaping macrophage function during the metastatic spread of cancer.

A growing number of studies have highlighted the importance of metabolism in dictating macrophage activation and function.[25–29] However, a large number of contradictory observations have complicated their interpretation, possibly caused by fundamental differences between *in vitro* and *in vivo* experimental settings and the fact that the binary anti-tumor or ''M1-like'' versus pro-tumor ''M2-like'' polarization model does not accurately reflect the heterogeneity of macrophages, especially in the context of cancer.[30–32] For example, mTORC1-driven differentiation of monocytes into M2-like tumor-associated macrophages (TAMs) was found to promote angiogenesis and tumor growth in a liver cancer model.[33] In contrast, Wenes et al. reported that activation of mTORC1–through deletion of REDD1–in hypoxic TAMs enhanced a switch to glycolysis, normalized the tumor vasculature restoring oxygenation, and prevented formation of metastasis.[34] Our data add another layer that might explain some of these seemingly conflicting results. Our

work shows that the initial ingestion of tumor-derived material induces rapid mTORC1 activation in macrophages driving metabolic programs characterized by enhanced oxidative phosphorylation that support an anti-metastatic function in the pre-metastatic lung (Figure 6G). However, this anti-tumor phenotype seems to be lost upon prolonged exposure to growing metastatic lesions (Figures S6D and S6E). It is plausible that the high metabolic demand of tumor cells in overt metastatic lungs enforces temporal changes in the local composition of oxygen and nutrients that result in spatiotemporal metabolic changes driving a shift in macrophage function from an anti-tumor to a pro-tumor state. Adding to the complexity, the metabolic changes in immune cells observed in tumor studies seem to be highly dependent on context, including the timing of experimental analysis and the type of pre-clinical cancer model used. For example, uptake of glioblastoma-derived material by microglia in the brain was shown to downregulate pathways involved in immune recognition, sensing of metabolic signals, and tumor cell killing and upregulate genetic programs that support tumor growth and invasion.[35,36] Our observation that ZsGreen⁺ macrophages downregulate expression of a ''DC signature'' (Figure 1D) is in line with these findings and suggests that uptake of tumor-derived material reprograms macrophages to a more pro-tumorigenic phenotype. The significant enrichment of metabolism-related pathways in our dataset might be caused by capturing the very early stages (24 h post-i.v. injection) of this reprogramming event. We expect that over time, with the tumor burden in the lung increasing, the macrophage phenotype will change and co-evolve with the establishment of an immunosuppressive tumor microenvironment (TME). Thus, further studies are needed to understand how macrophage function is shaped by changes in metabolic states over time in growing tumors.

Manipulation of macrophages has been an interesting avenue for therapeutic intervention to prevent or slow down tumor progression and metastatic spread in a substantial proportion of patients with cancer. However, the success of myeloid cell-targeting compounds in clinical trials has been limited.[37] A major caveat in developing macrophage-targeting compounds is most likely a lack of specificity caused by the extremely heterogeneous and plastic nature of these cells. Ideally, one would target pro-tumor macrophage states and leave the anti-tumor macrophages unaffected. Based on our study and others', it would be interesting to identify ways of targeting certain metabolic states in macrophages to selectively suppress the pro-tumor function of macrophages and enhance their anti-tumor function to work in conjunction with other anti-cancer therapies.

Limitations of the study

Here, we present that macrophages ingesting tumor-derived microparticles in the early metastatic lung undergo a functional reprogramming event that is characterized by increased mitochondrial metabolism. Refined studies are needed to determine whether these particles contain tumor-derived (damaged) mitochondria that could result in the increase in mTORC1-dependent metabolic processes in macrophages. Additionally, our study only covered the very early phases of interaction between disseminated tumor cells and macrophages in the lung. To take into account other environmental stimuli that are present in the developing metastatic TME, more elaborate studies are required to assess

the functional consequences of macrophage reprogramming at different time points during metastatic progression.

STAR★METHODS

RESOURCE AVAILABILITY

Lead contact—Further information and requests for resources and reagents should be directed to and will be fulfilled by the lead contact, Mark Headley (mheadley@fredhutch.org).

Materials availability—All unique reagents generated in this study are available from the lead contact without restriction.

Data and code availability

- Bulk Murine RNA-seq data are publicly available as of the date of publication (GEO accession code GSE230517.) Infinity Flow data are available as FCS files from Flow Repository (ID# FR-FCM-Z68V.) Accession numbers are also listed in the key resources table.

- No original code was written for analyses contained in this manuscript; all analyses were carried out using publicly available resources. DOIs are listed in the key resources table.

- Any additional information required to reanalyze the data reported in this paper is available from the lead contact upon request.

EXPERIMENTAL MODEL AND SUBJECT DETAILS

Mice—All mice were treated in accordance with the regulatory standards of the National Institutes of Health and American Association of Laboratory Animal Care and were approved by the UCSF Institution of Animal Care and Use Committee and were maintained under specific pathogen-free conditions at the University of California, San Francisco Animal Barrier Facility. C57BL/6J mice were purchased from The Jackson Laboratory. *MacBlue* mice were a gift from David Hume (The Roslin Institute). *Rptr*$^{f/f}$ and *Rctr*$^{f/f}$ mice (a gift from Xin Chen, UCSF) were bred to *LysM*^{Cre} mice (strain # 004781, The Jackson Laboratory) for >10 generations. MEFs were derived from *Ai6;β*-actin^{Cre} mice that were generated by crossing *β*-actin^{Cre} (strain # 033984, The Jackson Laboratory) to *Ai6* mice (strain # 007906,The Jackson Laboratory) as previously described.[2] Both male and female mice ranging in age from 6 to 20 weeks were used for experimentation. Food and water were provided ad libitum.

Cell lines—B16F10-ZsGreen cells were previously generated in our laboratory as described.[2] B16F1-ZsGreen and Lewis Lung Carcinoma (LLC)-ZsGreen cells were generated through transduction of B16F1 or LLC with empty pSiren-ZsGreen (Clontech). All cells were cultured under standard conditions 37°C in 5% CO2 in DMEM (GIBCO), 10% FCS (Benchmark), 1% Pen/Strep/Glut (Invitrogen) unless stated otherwise.

METHOD DETAILS

Cell line intravenous injections—Adherent tumor cells or MEFs were grown to confluency and harvested using 0.05% Trypsin-EDTA (GIBCO) and washed 3x with PBS (GIBCO). For studies involving acute responses, $5–10\times10^5$ cells were injected intravenously (i.v.) via the tail vein in a final volume of 100μL PBS and mice were euthanized 24 h later. For uptake of beads, 1×10^9 FITC-labeled polystyrene beads (Sigma) were resuspended in 100μL PBS and injected i.v. and mice were euthanized 24 h later. For long-term metastasis experiments, 1.5×10^5 B16ZsGreen cells in PBS were injected i.v. and mice were euthanized 2–3 weeks later and lungs were harvested for analysis.

Rapamycin treatment *in vivo*—Rapamycin (Millipore Sigma) at 0.4 mg per kg was delivered intranasally into mice one day prior to and 1 h post i.v. administration of B16ZsGreen. Mice were euthanized 24 h later and lungs were harvested for analysis.

Mouse lung digestion—Lungs were collected from mice following euthanasia by overdose with 2.5% Avertin. Lungs were placed in 3 mL of DMEM (GIBCO) in C-Tubes (Miltenyi) briefly processed with a GentleMACS Dissociator (Miltenyi). 2 mL of DMEM with 0.26 U ml^{-1} LiberaseTM (Roche) and 0.25 mg mL^{-1} DNase I (Roche) was subsequently added and samples were then incubated at 37°C in a shaker for 30 min and dissociated to single cell suspensions by GentleMACS. Tissue homogenate was then passed through a 100 μm filter. Red blood cells were lysed with 3 mL of 175 mM NH4Cl per lung for 5 min at room temperature. Samples were then washed with FACS buffer (2% FBS in PBS) and resuspended in appropriate buffer for staining for flow cytometry or FACS-sorting.

Flow cytometry and fluorescence-activated cell sorting—For flow cytometric analyses, cells were washed with PBS prior to staining with Zombie NIR Fixable live/dead dye (Biolegend) for 20 min at 4°C. Cells were washed in PBS followed by surface staining for 30 min at 4°C with directly conjugated antibodies diluted in FACS buffer containing anti-CD16/32 (clone 2.4G2; BioXCell) to block non-specific binding. Cells were washed again with FACS buffer. For intracellular staining, cells were fixed for 20 min at 4°C using the FOXP3 Fix/Perm kit (BD Biosciences), and washed in permeabilization buffer. Antibodies against intracellular targets were diluted in permeabilization buffer and cells were incubated for 30 min at 4°C followed by another wash prior to readout on a BD LSR Fortessa SORP cytometer.

For FACS-sorting, cells were washed in PBS followed by surface staining for 30 min at 4°C with directly conjugated antibodies diluted in FACS buffer containing anti-CD16/32. Cells were washed with FACS buffer and filtered over a 70μm mesh. Immediately prior to sorting, DAPI was added to exclude dead cells. Cells were sorted on a BD FACSAria Fusion and BD FACSAria2. Sorted myeloid cells were collected in DMEM (GIBCO), 10% FCS (Benchmark), Pen/Strep/Glut (Invitrogen) at 4°C for further use *ex vivo.*

For mitochondrial analysis, Mitotracker Deep Red FM (Invitrogen) at 200nM and TMRM (Thermo Fisher Scientific) at 100nM were used for staining of lung cells for the detection of mitochondrial mass and membrane potential. Cells were stained with Mitotracker and TMRM in DMEM at 37°C for 30 min before staining with surface antibodies.

RNA sequencing—ZsGreen$^+$ and ZsGreen$^-$ macrophages were isolated from lungs of mice 24 h post i.v. injection with B16ZsGreen. Cells were double sorted to ensure high purity. 200 cells were isolated for each sample with 4 biological replicates. Cells were sorted directly into 100ul of Arcturus PicoPure Lysis Buffer. RNA was prepared using the Arcturus PicoPure RNA Isolation Kit (ThermoFisher). Libraries were prepared for each sample utilizing the Nugen Ovation Library Preparation Kit (Tecan). Single End 50bp sequencing was performed on an Illumina HiSeq 3000. Data were aligned to the *Mus musculus* Ensembl GRCm38 v.78 genome and those reads uniquely mapping to Ensembl IDs were tabulated using STAR_2.4.2a. The resulting sample by gene matrix was passed to DESeq2 for downstream normalization and differential expression testing.

Pathway enrichment analysis—For gene set enrichment analysis of samples derived from ZsGreen$^+$ and ZsGreen$^-$ macrophages, log2 fold changes between groups were calculated for each protein coding gene that was expressed at greater than 5 counts per million (cpm). The resulting, ordered list was passed to the GSEApreRanked function, implemented in GSEA software, downloaded from the Broad Institute (www.gsea-msigdb.org/gsea/index.jsp). GSEApreRanked was run with default parameters on both Hallmark and c5 gene set collections contained in the Broad's Molecular Signatures Database (MSigDB). Results from the c5 gene set were passed to Cytoscape (www.cytoscape.org) software (v3.71) which was run using default parameters to generate pathway network plots.

Infinity flow—Infinity Flow was performed as previously described.[10] Briefly, single cell suspensions of mouse lungs were washed with PBS prior to staining with Zombie NIR Fixable live/dead dye (Biolegend) for 20 min at room temperature (RT). Following staining, a 10-fold volume of Cell Staining Buffer (BioLegend) was added to neutralize any unbound dye and cells were centrifuged at 300g for 5 min. Cells were resuspended at 20×10^6 cells/ml in Cell Staining Buffer, and nonspecific staining was then blocked by addition of anti-CD16/32 (2 μg/mL; mouse TrueStain FcX, BioLegend), 2% rat serum (Invitrogen), and 2% Armenian hamster serum (Innovative Research) followed by 15 min incubation at 4°C. Cells were then washed, resuspended in Cell Staining Buffer and a master mix of the indicated Backbone antibody panel[10] at 20×10^6 cells/ml, and incubated for 30 min at 4°C. Following Backbone staining, cells were washed twice and resuspended at 20×10^6 cells/ml in Cell Staining Buffer and 75 μL was added to each well of the LEGENDScreen plates. Staining and fixation were performed exactly as per manufacturer directions. Note a portion of the dataset described, here in Figure 1, was published in[9] alongside the Infinity Flow method. This data represents an expanded dataset and the analysis is non-overlapping. These data are available for download from FlowRepository (Repository ID: FR-FCM-Z68V).

Two photon imaging of mouse lung slices and analysis—Slice imaging was performed as previously described.[2] Briefly, *MacBlue* mice were injected with 1×10^6 B16ZsGreen cells through the tail vein. After 24 h, mice were euthanized by anesthetic overdose with 1 mL 2.5% Avertin and then intubated by tracheotomy with the sheath from an 18-gauge i.v. catheter. Lungs were subsequently inflated with 1 mL of 2% low melting agarose (BMA) in sterile PBS at 37°C. Agarose was then solidified by flooding

the chest cavity with 4°C PBS. Inflated lungs were excised, and the left lobe was cut into 250μm sections using a vibratome. Sections were mounted on plastic coverslips and imaged by two-photon microscopy at 37°C in carbogen (5% CO_2:95% O_2)-perfused RPMI-1640 media (GIBCO, without Phenol Red) in a heated chamber. The Maitai laser of two-photon microscope was set to 800nm for excitation of CFP. The Chameleon laser was set to 950nm for excitation of ZsGreen. Emitted light was detected using a 25x 1.2NA water lens (Zeiss) coupled to a 6-color detector array (custom; using Hamamatsu H9433MOD detectors). Emission filters used were blue 475/23, green 510/42, yellow 542/27, red 607/70, far red 675/67. The microscope was controlled by the MicroManager software suite, and time-lapse z stack images were acquired every 90 s with five-fold averaging and z-step of 4μm. Data analysis was performed with Imaris software (Bitplane).

Bone marrow-derived macrophage (BMDM) and B16ZsGreen coculture—Bone marrow was obtained from femurs and tibia of C57BL6/J mice and cultured in DMEM (GIBCO), 10% FCS (Benchmark), Pen/Strep/Glut (Invitrogen) in the presence of 20 ng/ml M-CSF (Peprotech) for 5 days. BMDM were then co-cultured with B16ZsGreen cells at a 5:1 ratio for 24 h before assays.

Extracellular flux analysis—Extracellular flux was measured using a Seahorse XFe24 or XFe96 Analyzer (Agilent) using Mito Stress Test Kits (Aligent Technologies) per manufacturer instructions. Sorted CD11b$^+$ BMDM or lung macrophages were plated in poly-L-lysine-coated XFe24 or XFe96 plates for 1 h before the assay. Respiration was measured in the basal state and in response to 1μM oligomycin, 1μM FCCP and 0.5μM rotenone and antimycin A.

Quantification of ATP luminescence—ATP production from FACS-sorted lung macrophages was measured using Luminescent ATP Detection Assay Kit (Abcam) per manufacturer instructions. Lung macrophages were plated in poly-L-lysine-coated 96 flat bottom plates 1 h prior to ATP detection. Luminescence was measured using FlexStation 3 Multi-Mode Microplate Reader (Molecular Devices).

Metabolic tracing of isotopically labeled ^{13}C-glucose—BMDM and B16ZsGreen co-culture was performed as noted above. After 24 h, cells were collected and FACS-sorted based on ZsGreen-positivity (ZsGreen$^-$, ZsGreen$^+$ and non-tumor challenged (NT)). X cells were cultured in xx flat bottom plates and allowed to rest for 1 h in D10. The medium was exchanged for DMEM medium containing 25 mM ^{13}C-glucose (Cambridge Isotope Laboratories Inc., CLM-1396) and no additional ^{12}C-glucose for 2 h. Cells were washed twice with PBS and extracted with mass spectrometry grade 80% methanol (ThermoFisher, A456–1) and 20% water (ThermoFisher, W6500) supplemented with 5 nmol DL-Norvaline (Sigma, N7502). Protein concentrations of the methanol extract were determined via BCA (Pierce, 23225) with no significant variability assessed (5 μL transferred into 45 μL RIPA buffer, 5 μL of the RIPA dissolved solution assayed). Insoluble material was pelleted in a 4°C centrifuge at 16,000g, the supernatant was transferred and dried in a Speedvac. Dried metabolites were resuspended in 50% ACN:water and 1/10th of the volume was loaded onto a Luna 3 μm NH2 100A (150 × 2.0 mm) column (Phenomenex). The chromatographic

separation was performed on a Vanquish Flex (Thermo Scientific) with mobile phases A (5 mM NH_4AcO pH 9.9) and B (ACN) and a flow rate of 200 μL/min. A linear gradient from 15% A to 95% A over 18 min was followed by 9 min isocratic flow at 95% A and re-equilibration to 15% A. Metabolites were detected with a Thermo Scientific Q Exactive mass spectrometer run with polarity switching (+3.5 kV/⁻3.5 kV) in full scan mode with an m/z range of 65–975. TraceFinder 4.1 (Thermo Scientific) was used to quantify the targeted metabolites by area under the curve using expected retention time and accurate mass measurements (<5 ppm). Values were normalized to cell number and sample protein concentration. Relative amounts of metabolites were calculated by summing up the values for all isotopologues of a given metabolite. Fractional contribution (FC) of ^{13}C carbons to total carbon for each metabolite was calculated.[38] Data analysis was performed using in-house developed R scripts.

Quantification of metastatic burden—Metastatic seeding: The proportion of CD45⁻ZsGreen⁺ cells was gated of total live cells from total lung single cell suspensions 24 h after i.v. administration of $5–10 \times 10^5$ B16ZsGreen cells using flow cytometry.

Overt metastatic disease: The number of metastatic foci on the surface of all the lobes were counted by eye by two blinded researchers under a dissection microscope. The left lobe was fixed in 4% PFA and processed into formalin-fixed paraffin-embedded tissue blocks. One section was stained in H&E and the total area of the lung affected by metastasis was quantified by manually outlining metastatic nodules and total lung lobe in ImageJ. The metastatic burden was calculated as the percentage of area affected by metastatic nodules as a fraction of the total lung lobe area.

QUANTIFICATION AND STATISTICAL ANALYSIS

Statistical analysis—Unless specifically noted, all data are representative of ≥2 separate experiments. Experimental group assignment was determined by random designation. Statistical analyses were performed using GraphPad Prism software. Error bars represent ±standard error of the mean (S.E.M.) calculated using Prism. Specific statistical tests used were paired and unpaired Student's t-tests, Mann-Whitney U-test, and two-way ANOVA as specified in the figure legends. p-values <0.05 were considered statistically significant. Investigators were not blinded to group assignment during experimental procedures or analysis.

Supplementary Material

Refer to Web version on PubMed Central for supplementary material.

ACKNOWLEDGMENTS

REFERENCES

1. Kitamura T, Qian B-Z, and Pollard JW (2015). Immune cell promotion of metastasis. Nat. Rev. Immunol 15, 73–86. 10.1038/nri3789. [PubMed: 25614318]

2. Headley MB, Bins A, Nip A, Roberts EW, Looney MR, Gerard A, and Krummel MF (2016). Visualization of immediate immune responses to pioneer metastatic cells in the lung. Nature 531, 513–517. 10.1038/nature16985. [PubMed: 26982733]

3. DeNardo DG, and Ruffell B (2019). Macrophages as regulators of tumour immunity and immunotherapy. Nat. Rev. Immunol 19, 369–382. 10.1038/s41577-019-0127-6. [PubMed: 30718830]

4. Hanna RN, Cekic C, Sag D, Tacke R, Thomas GD, Nowyhed H, Herrley E, Rasquinha N, McArdle S, Wu R, et al. (2015). Patrolling monocytes control tumor metastasis to the lung. Science 350, 985–990. 10.1126/science.aac9407. [PubMed: 26494174]

5. Morrissey SM, Zhang F, Ding C, Montoya-Durango DE, Hu X, Yang C, Wang Z, Yuan F, Fox M, Zhang H-G, et al. (2021). Tumor-derived exosomes drive immunosuppressive macrophages in a pre-metastatic niche through glycolytic dominant metabolic reprogramming. Cell Metab 33, 2040–2058. [PubMed: 34559989]

6. Costa-Silva B, Aiello NM, Ocean AJ, Singh S, Zhang H, Thakur BK, Becker A, Hoshino A, Mark MT, Molina H, et al. (2015). Pancreatic cancer exosomes initiate pre-metastatic niche formation in the liver. Nat. Cell Biol 17, 816–826. 10.1038/ncb3169. [PubMed: 25985394]

7. Hoshino A, Costa-Silva B, Shen T-L, Rodrigues G, Hashimoto A, Tesic Mark M, Molina H, Kohsaka S, Di Giannatale A, Ceder S, et al. (2015). Tumour exosome integrins determine organotropic metastasis. Nature 527, 329–335. 10.1038/nature15756. [PubMed: 26524530]

8. Peinado H, Ale kovi M, Lavotshkin S, Matei I, Costa-Silva B, Moreno-Bueno G, Hergueta-Redondo M, Williams C, García-Santos G, Ghajar C, et al. (2012). Melanoma exosomes educate bone marrow progenitor cells toward a pro-metastatic phenotype through MET. Nat. Med 18, 883–891. 10.1038/nm.2753. [PubMed: 22635005]

9. Minciacchi VR, Freeman MR, and Di Vizio D (2015). Extracellular vesicles in cancer: exosomes, microvesicles and the emerging role of large oncosomes. Semin. Cell Dev. Biol 40, 41–51. 10.1016/j.semcdb.2015.02.010. [PubMed: 25721812]

10. Becht E, Tolstrup D, Dutertre C-A, Morawski PA, Campbell DJ, Ginhoux F, Newell EW, Gottardo R, and Headley MB (2021). High-throughput single-cell quantification of hundreds of proteins using conventional flow cytometry and machine learning. Sci. Adv 7, eabg0505. 10.1126/sciadv.abg0505. [PubMed: 34550730]

11. Barry KC, Hsu J, Broz ML, Cueto FJ, Binnewies M, Combes AJ, Nelson AE, Loo K, Kumar R, Rosenblum MD, et al. (2018). A natural killer-dendritic cell axis defines checkpoint therapy-responsive tumor microenvironments. Nat. Med 24, 1178–1191. 10.1038/s41591-018-0085-8. [PubMed: 29942093]

12. Broz ML, Binnewies M, Boldajipour B, Nelson AE, Pollack JL, Erle DJ, Barczak A, Rosenblum MD, Daud A, Barber DL, et al. (2014). Dissecting the tumor myeloid compartment reveals rare activating antigen-presenting cells critical for T cell immunity. Cancer Cell 26, 638–652. 10.1016/j.ccell.2014.09.007. [PubMed: 25446897]

13. Ovchinnikov DA, van Zuylen WJM, DeBats CEE, Alexander KA, Kellie S, and Hume DA (2008). Expression of Gal4-dependent transgenes in cells of the mononuclear phagocyte system labeled with enhanced cyan fluorescent protein using Csf1r-Gal4VP16/UAS-ECFP double-transgenic mice. J. Leukoc. Biol 83, 430–433. 10.1189/jlb.0807585. [PubMed: 17971498]

14. Cunningham JT, Rodgers JT, Arlow DH, Vazquez F, Mootha VK, and Puigserver P (2007). mTOR controls mitochondrial oxidative function through a YY1-PGC-1alpha transcriptional complex. Nature 450, 736–740. 10.1038/nature06322. [PubMed: 18046414]

15. Morita M, Gravel S-P, Chénard V, Sikström K, Zheng L, Alain T, Gandin V, Avizonis D, Arguello M, Zakaria C, et al. (2013). mTORC1 controls mitochondrial activity and biogenesis through

4E-BP-dependent translational regulation. Cell Metab 18, 698–711. 10.1016/j.cmet.2013.10.001. [PubMed: 24206664]

16. Covarrubias AJ, Aksoylar HI, Yu J, Snyder NW, Worth AJ, Iyer SS, Wang J, Ben-Sahra I, Byles V, Polynne-Stapornkul T, et al. (2016). Akt-mTORC1 signaling regulates Acly to integrate metabolic input to control of macrophage activation. Elife 5, e11612. 10.7554/eLife.11612. [PubMed: 26894960]

17. Huang SC-C, Smith AM, Everts B, Colonna M, Pearce EL, Schilling JD, and Pearce EJ (2016). Metabolic reprogramming mediated by the mTORC2-IRF4 signaling Axis is essential for macrophage alternative activation. Immunity 45, 817–830. 10.1016/j.immuni.2016.09.016. [PubMed: 27760338]

18. Hallowell RW, Collins SL, Craig JM, Zhang Y, Oh M, Illei PB, Chan-Li Y, Vigeland CL, Mitzner W, Scott AL, et al. (2017). mTORC2 signalling regulates M2 macrophage differentiation in response to helminth infection and adaptive thermogenesis. Nat. Commun 8, 14208. 10.1038/ncomms14208. [PubMed: 28128208]

19. Weichhart T, Hengstschläger M, and Linke M (2015). Regulation of innate immune cell function by mTOR. Nat. Rev. Immunol 15, 599–614. 10.1038/nri3901. [PubMed: 26403194]

20. Jang C, Chen L, and Rabinowitz JD (2018). Metabolomics and isotope tracing. Cell 173, 822–837. 10.1016/j.cell.2018.03.055. [PubMed: 29727671]

21. . Joyce JA, and Pollard JW (2009). Microenvironmental regulation of metastasis. Nat. Rev. Cancer 9, 239–252. 10.1038/nrc2618. [PubMed: 19279573]

22. Güç E, and Pollard JW (2021). Redefining macrophage and neutrophil biology in the metastatic cascade. Immunity 54, 885–902. 10.1016/j.immuni.2021.03.022. [PubMed: 33979586]

23. Gener Lahav T, Adler O, Zait Y, Shani O, Amer M, Doron H, Abramovitz L, Yofe I, Cohen N, and Erez N (2019). Melanoma-derived extracellular vesicles instigate proinflammatory signaling in the metastatic microenvironment. Int. J. Cancer 145, 2521–2534. 10.1002/ijc.32521. [PubMed: 31216364]

24. Crewe C, Funcke J-B, Li S, Joffin N, Gliniak CM, Ghaben AL, An YA, Sadek HA, Gordillo R, Akgul Y, et al. (2021). Extracellular vesicle-based interorgan transport of mitochondria from energetically stressed adipocytes. Cell Metab 33, 1853–1868.e11. 10.1016/j.cmet.2021.08.002. [PubMed: 34418352]

25. Van den Bossche J, O'Neill LA, and Menon D (2017). Macrophage immunometabolism: where are we (going)? Trends Immunol 38, 395–406. 10.1016/j.it.2017.03.001. [PubMed: 28396078]

26. Mazzone M, Menga A, and Castegna A (2018). Metabolism and TAM functions-it takes two to tango. FEBS J 285, 700–716. 10.1111/febs.14295. [PubMed: 29055087]

27. Vitale I, Manic G, Coussens LM, Kroemer G, and Galluzzi L (2019). Macrophages and metabolism in the tumor microenvironment. Cell Metab 30, 36–50. 10.1016/j.cmet.2019.06.001. [PubMed: 31269428]

28. Argüello RJ, Combes AJ, Char R, Gigan J-P, Baaziz AI, Bousiquot E, Camosseto V, Samad B, Tsui J, Yan P, et al. (2020). SCENITH: a flow cytometry-based method to functionally profile energy metabolism with single-cell resolution. Cell Metab 32, 1063–1075.e7. 10.1016/j.cmet.2020.11.007. [PubMed: 33264598]

29. Li S, Yu J, Huber A, Kryczek I, Wang Z, Jiang L, Li X, Du W, Li G, Wei S, et al. (2022). Metabolism drives macrophage heterogeneity in the tumor microenvironment. Cell Rep 39, 110609. 10.1016/j.celrep.2022.110609. [PubMed: 35385733]

30. Artyomov MN, Sergushichev A, and Schilling JD (2016). Integrating immunometabolism and macrophage diversity. Semin. Immunol 28, 417–424. 10.1016/j.smim.2016.10.004. [PubMed: 27771140]

31. Laviron M, Petit M, Weber-Delacroix E, Combes AJ, Arkal AR, Barthélémy S, Courau T, Hume DA, Combadière C, Krummel MF, Boissonnas A (2022). Tumor-associated macrophage heterogeneity is driven by tissue territories in breast cancer. Cell Rep 39, 110865. 10.1016/j.celrep.2022.110865. [PubMed: 35613577]

32. Mujal AM, Combes AJ, Rao AA, Binnewies M, Samad B, Tsui J, Boissonnas A, Pollack JL, Argu€ello, R.J., Meng, M.V., et al. (2022). Holistic characterization of tumor monocyte-

to-macrophage differentiation Integrates distinct immune phenotypes in kidney cancer. Cancer Immunol. Res 10, 403–419. 10.1158/2326-6066.CIR-21-0588. [PubMed: 35181780]

33. Chen W, Ma T, Shen X.n., Xia X.f., Xu G.d., Bai X.l., and Liang T.b. (2012). Macrophage-induced tumor angiogenesis is regulated by the TSC2-mTOR pathway. Cancer Res 72, 1363–1372. 10.1158/0008-5472.CAN-11-2684. [PubMed: 22287548]

34. Wenes M, Shang M, Di Matteo M, Goveia J, Martín-Pérez R, Serneels J, Prenen H, Ghesquière B, Carmeliet P, and Mazzone M (2016). Macrophage metabolism controls tumor blood vessel morphogenesis and metastasis. Cell Metab 24, 701–715. 10.1016/j.cmet.2016.09.008. [PubMed: 27773694]

35. Abels ER, Maas SLN, Nieland L, Wei Z, Cheah PS, Tai E, Kolsteeg C-J, Dusoswa SA, Ting DT, Hickman S, et al. (2019). Glioblastoma-associated microglia reprogramming is mediated by functional transfer of extracellular miR-21. Cell Rep 28, 3105–3119.e7. 10.1016/j.celrep.2019.08.036. [PubMed: 31533034]

36. Maas SLN, Abels ER, Van De Haar LL, Zhang X, Morsett L, Sil S, Guedes J, Sen P, Prabhakar S, Hickman SE, et al. (2020). Glioblastoma hijacks microglial gene expression to support tumor growth. J. Neuroinflammation 17, 120. 10.1186/s12974-020-01797-2. [PubMed: 32299465]

37. Pittet MJ, Michielin O, and Migliorini D (2022). Clinical relevance of tumour-associated macrophages. Nat. Rev. Clin. Oncol 19, 402–421. 10.1038/s41571-022-00620-6. [PubMed: 35354979]

38. Cameron AM, Castoldi A, Sanin DE, Flachsmann LJ, Field CS, Puleston DJ, Kyle RL, Patterson AE, Hässler F, Buescher JM, et al. (2019). Inflammatory macrophage dependence on NAD+ salvage is a consequence of reactive oxygen species-mediated DNA damage. Nat. Immunol 20, 420–432. 10.1038/s41590-019-0336-y. [PubMed: 30858618]

Highlights

- Ingestion of tumor-derived material induces phenotypic reprogramming in macrophages

- Macrophage reprogramming impacts patrolling behavior in response to tumor cells

- ZsGreen+ macrophages show enhanced mitochondrial metabolism characterized by OXPHOS

- mTORC1 is required for enhanced OXPHOS and ATP production in ZsGreen+ macrophages
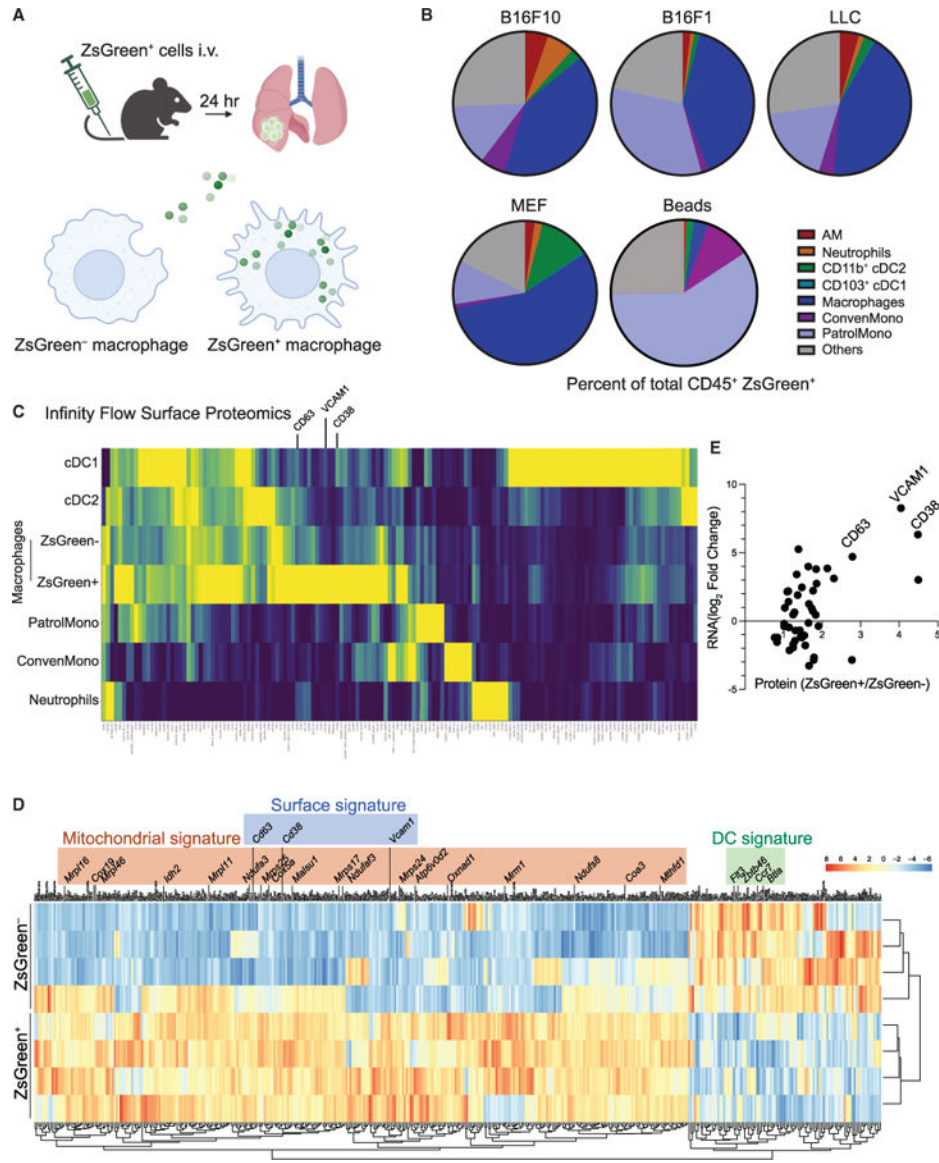
Figure 1. Uptake of tumor-derived microparticles induces transcriptional and phenotypic reprogramming of macrophages in the early metastatic lung

(A) Schematic overview of experimental setup. Lungs were harvested 24 h post-i.v. administration of ZsGreen$^+$ cells in the tail vein.

(B) Quantification of flow cytometric analysis of the uptake of ZsGreen$^+$ microparticles by distinct CD45$^+$ myeloid cell populations in the lung 24 h post-i.v. injection of cancer cells (B16F10, B16F1, or Lewis lung carcinoma [LLC]), mouse embryonic fibroblasts (MEFs), or FITC-labeled polystyrene beads.

(C) Heatmap displaying differential expression of surface protein markers on myeloid cell populations in the lung 24 h post-i.v. injection of B16ZsGreen cells using Infinity Flow surface proteomics.

(D) Heatmap displaying the top differentially expressed genes (DEGs) in ZsGreen$^+$ and ZsGreen$^−$ macrophages isolated from lungs of mice 24 h post-i.v. injection of B16ZsGreen cells as described in (A). DEGs related to mitochondria (''mitochondrial signature''),

cellular adhesion markers (''surface signature''), and dendritic cell functions (''DC signature'') are color coded separately. n = 4 per group. DEGs were selected based on cutoff of false discovery rate (FDR) <0.05.

(E) Correlation between proteomics (ratio of ZsGreen$^+$/ZsGreen$^-$) and RNA expression (log$_2$ fold change) data in lung macrophages.

See also Figure S1.
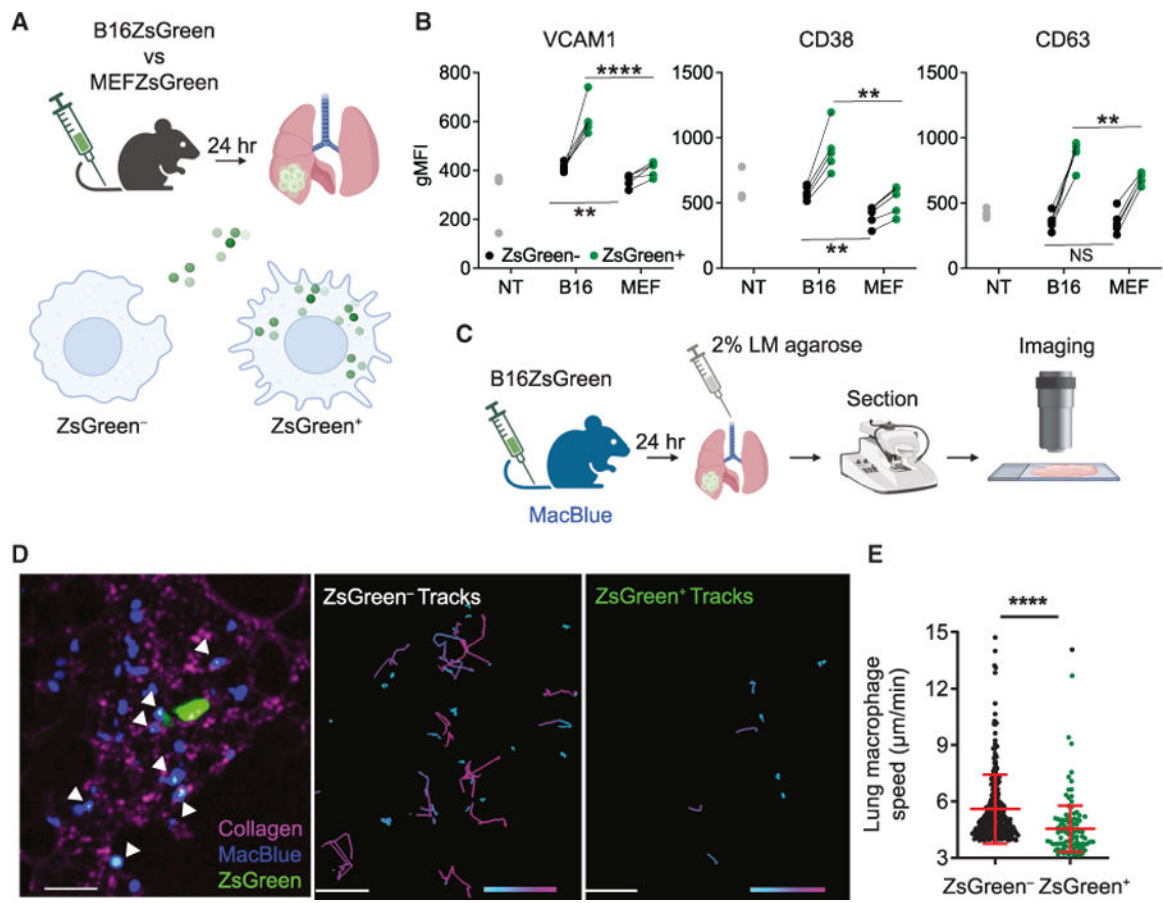
Figure 2. Ingestion of tumor-derived microparticles induces phenotypic reprogramming of macrophages in the early metastatic lung

(A) Schematic overview of experimental setup. Lungs were harvested 24 h post-i.v. administration of B16ZsGreen^{+} cells or MEFZsGreen^{+} cells in the tail vein.

(B) Quantification of VCAM1, CD38, and CD63 in ZsGreen[−] and ZsGreen[+] lung macrophages 24 h post-i.v. injection of B16ZsGreen (B16) or MEFZsGreen (MEF) by flow cytometry.

(C) Experimental layout of live precision-cut tissue slice imaging of lungs of MacBlue mice harvested post-i.v. injection of B16ZsGreen.

(D) Representative image and track displacement display of ZsGreen[+] versus ZsGreen[−] ECFP^{+} cells over 1 h in live lung slices from MacBlue mice at 24 h post-i.v. injection of B16ZsGreen cells. White arrows indicate ZsGreen-microparticle-ingested ECFP^{+} cells. Track length ranges from 3 (cyan) to 35 μm (pink). Scale bar: 40 μm.

(E) Quantification of the instant speed of ECFP^{+} cells in live lung slices.

Data are pooled from three different regions of interest (ROIs) and are representative of two independent experiments. ****$p < 0.0001$, **$p < 0.01$ as determined by Student's t test. See also Figures S2–S4.
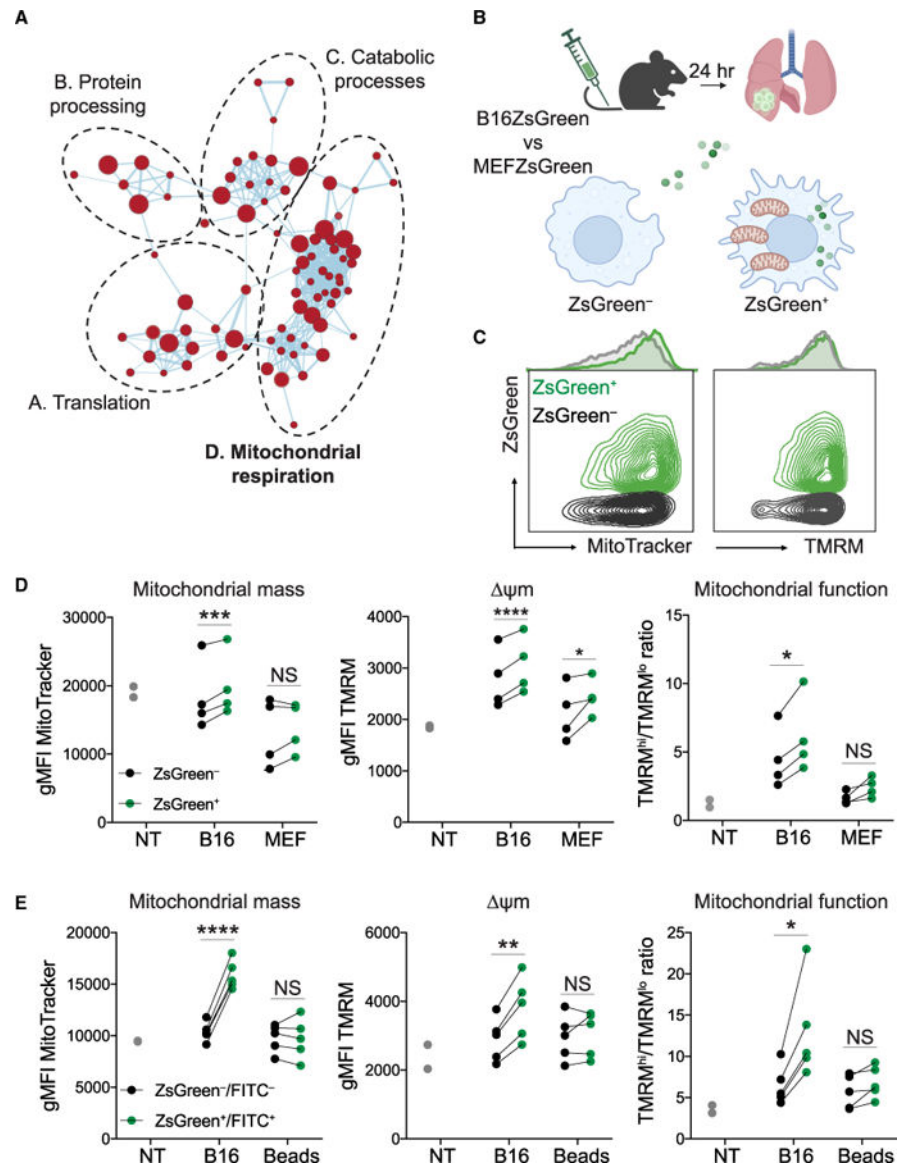
Figure 3. Tumor-derived antigen loading drives mitochondrial reprogramming in lung macrophages

(A) Cytoscape network analysis of enriched pathways in ZsGreen+ versus ZsGreen− lung macrophages. Also see Table S1 for a list of the identity of pathways in each cluster.

(B) Schematic overview of experimental setup. Lungs were harvested 24 h post-i.v. injection of B16ZsGreen or MEFZsGreen in the tail vein.

(C) Representative contour plots and histograms of MitoTracker DeepRed and TMRM staining of ZsGreen+ and ZsGreen− lung macrophages.

(D and E) Quantification of mitochondrial mass (MitoTracker DeepRed), mitochondrial membrane potential (TMRM), and mitochondrial function (ratio of the percentage of TMRM^{hi} to TMRM^{lo} cells) in ZsGreen− and ZsGreen+ lung macrophages 24 h post-i.v. injection of B16ZsGreen (B16), MEFZsGreen (MEF), FITC-labeled polystyrene beads (Beads), or non-tumor-challenged (NT) mice.

Data are representative of two or three independent experiments; ****p < 0.0001, ***p < 0.001, **p < 0.01, *p < 0.05 as determined by the paired Student's t test.

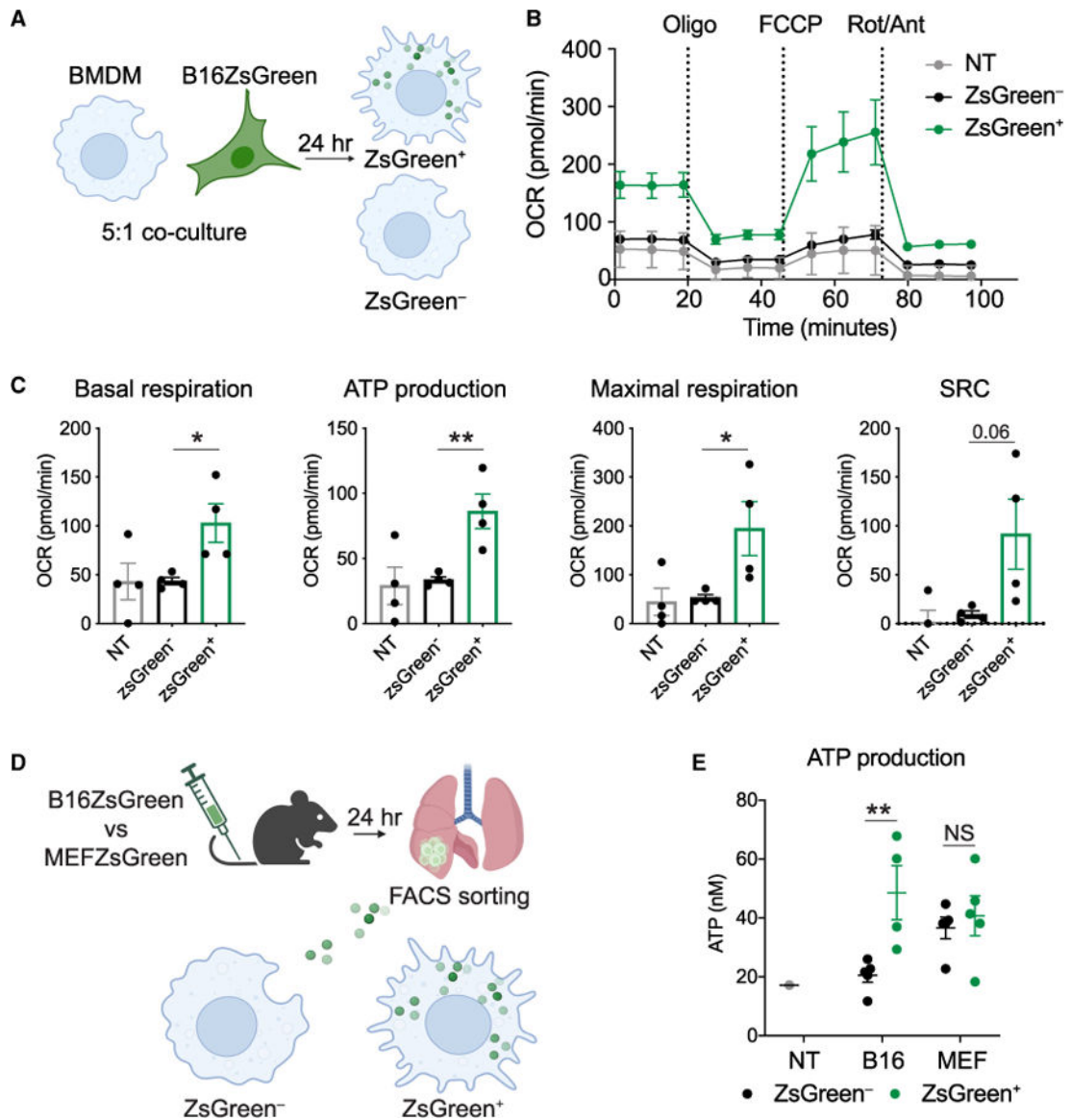**Figure 4. Metabolic reprogramming of lung macrophages upon ingestion of tumor-derived microparticles is characterized by enhanced oxidative phosphorylation**

(A) Schematic overview of experimental layout. Bone marrow-derived macrophages (BMDMs) and B16ZsGreen cells were co-cultured in 5:1 ratio for 24 h, after which CD11b^{+} ZsGreen^{−}, ZsGreen^{+}, or NT BMDMs were isolated using FACS and used for downstream analysis.

(B) FACS CD11b^{+} ZsGreen^{−}, ZsGreen^{+}, and NT BMDMs were plated into Seahorse XFe24 plates, and the oxygen consumption rate (OCR) was determined using Seahorse extracellular flux assay with oligomycin (Oligo), FCCP, and rotenone and antimycin A (Rot/Ant) added sequentially.

(C) Quantification of basal respiration, ATP production, maximal respiration, and spare respiratory capacity (SRC) from extracellular flux assay.

(D) Schematic overview of experimental layout of isolation of ZsGreen$^-$ and ZsGreen$^+$ macrophages from lungs harvested 24 h post-i.v. injection of B16ZsGreen or MEFZsGreen cells by FACS.

(E) Quantification of ATP production in FACS ZsGreen$^-$ and ZsGreen$^+$ macrophages described in (D) determined by luminescence detection per manufacturer instructions. Data are representative of two independent experiments; all data are represented as mean ± SEM; **$p < 0.01$, *$p < 0.05$ as determined by unpaired Student's t test (C) or two-way (E) ANOVA and Sidak's multiple comparison test.

See also Figure S5.
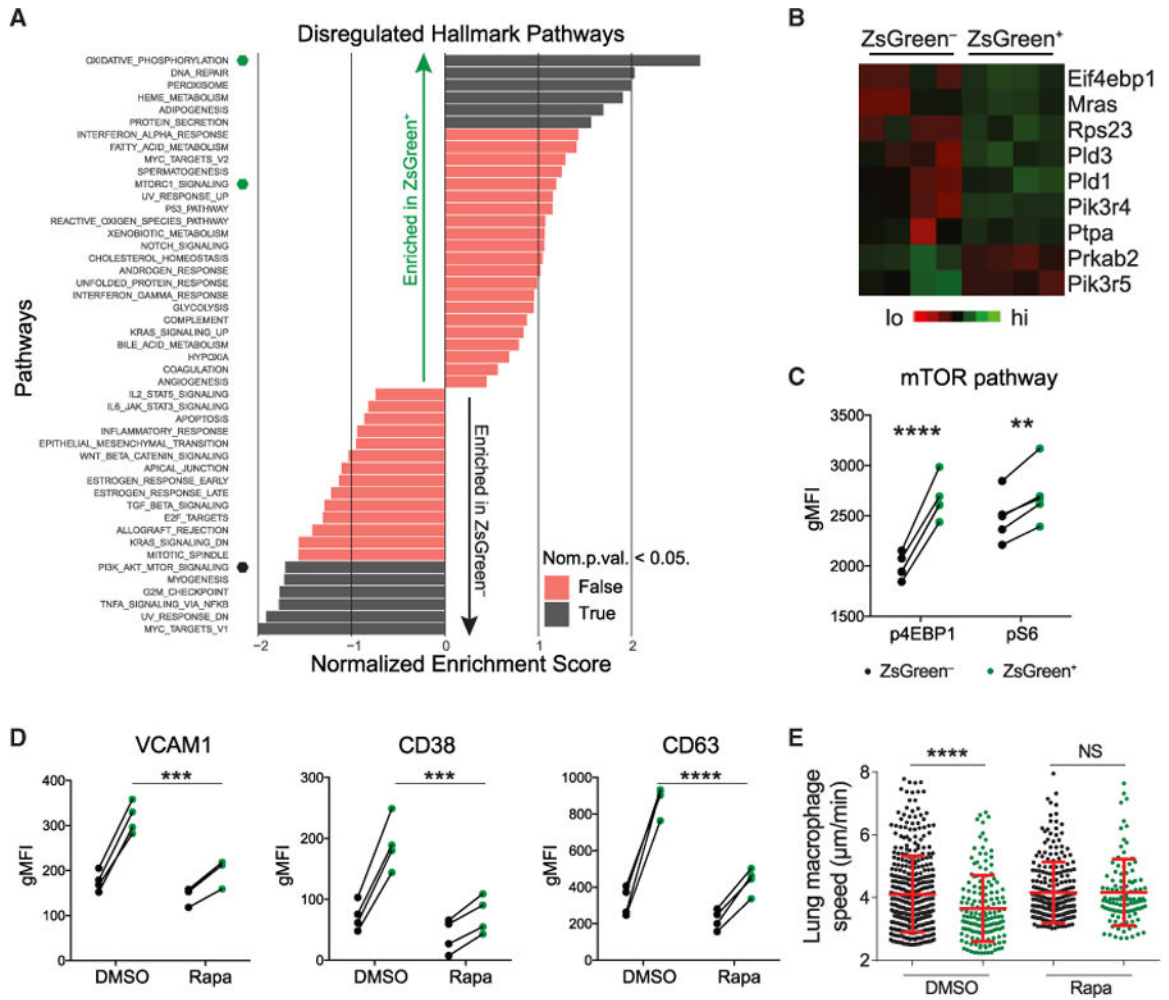
Figure 5. Phenotypic reprogramming of tumor microparticle-ingesting macrophages is mTORC1 dependent

(A) Hallmark pathway analysis showing pathways upregulated (normalized enrichment score > 0) or downregulated (normalized enrichment score < 0) in ZsGreen$^+$ versus ZsGreen$^-$ macrophages.

(B) Heatmap displaying expression of single DEGs in mTORC1 pathway in ZsGreen$^-$ versus ZsGreen$^+$ macrophages.

(C) Quantification of phospho-(p)4EBP1 and pS6 expression on ZsGreen$^-$ versus ZsGreen$^+$ macrophages 24 h post-i.v. injection of B16ZsGreen by intracellular flow cytometry.

(D) Quantification of VCAM1, CD38, and CD63 on ZsGreen$^-$ versus ZsGreen$^+$ lung macrophages harvested 24 h post-i.v. injection of B16ZsGreen. Intranasal DMSO or rapamycin (0.4 mg/kg) was administered twice, once on the day before and once on the day of tumor injection.

(E) Quantification of the instant speed of ZsGreen$^-$ versus ZsGreen$^+$ ECFP$^+$ cells in live lung slices from the same mice depicted in (D).

Data are pooled from three different ROIs for each group. Data are representative of two independent experiments; ****$p < 0.0001$, ***$p < 0.001$ as determined by paired Student's t

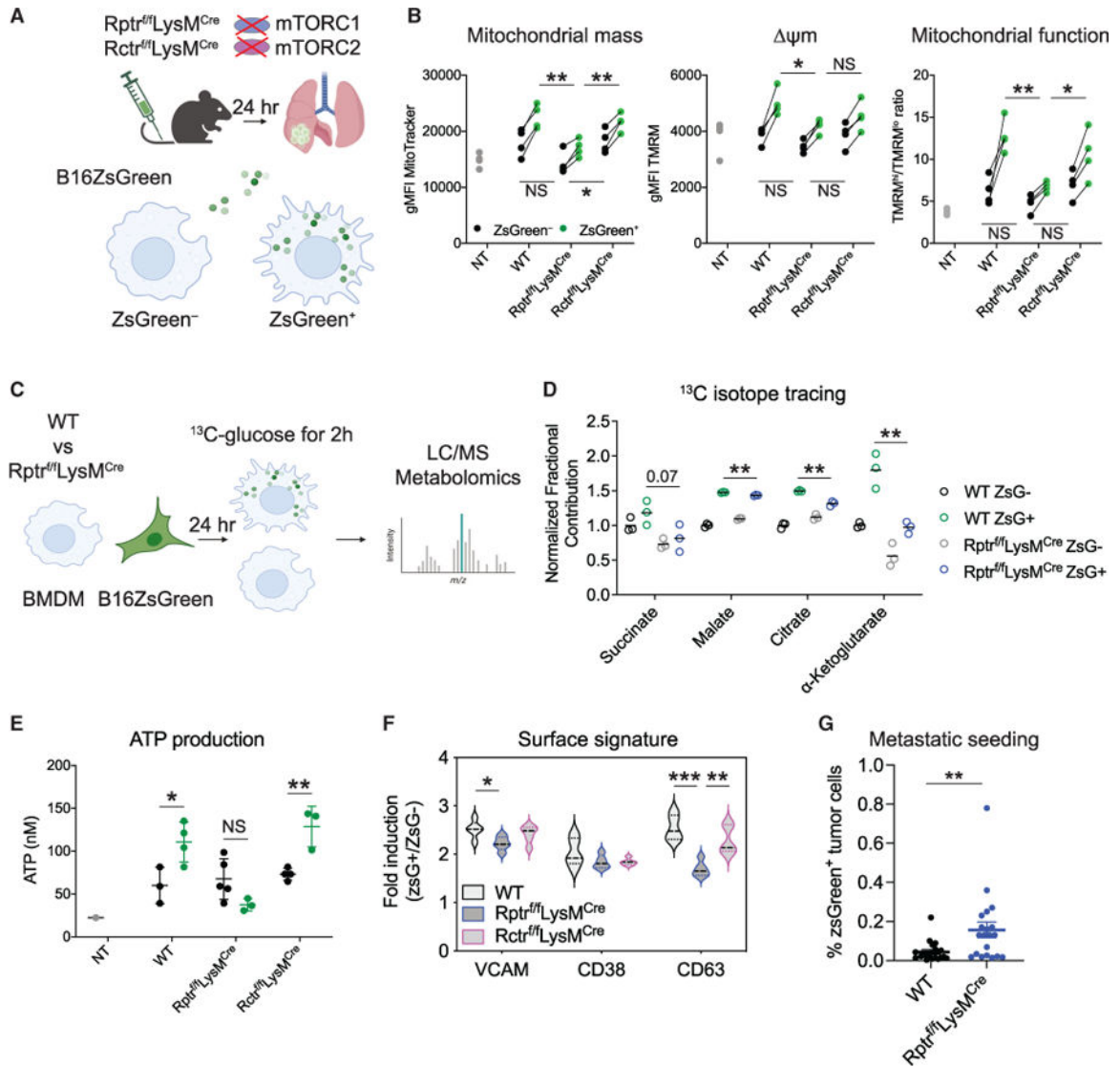test (C), two-way ANOVA and Sidak's multiple comparison test (D), and unpaired Student's t test (E).

Figure 6. mTORC1 is required for metabolic and phenotypic reprogramming of macrophages in the early metastatic lung

(A) Experimental layout of B16ZsGreen administration in mTORC1-deficient *Rptr^{f/f}/LysM^{Cre}*, mTORC2-deficient *Rctr^{f/f}/LysM^{Cre}* mice, and wild-type (WT) littermates.

(B) Quantification of mitochondrial mass (MitoTracker DeepRed), mitochondrial membrane potential (TMRM), and mitochondrial function (ratio of the percentage of TMRM^{hi} to TMRM^{lo} cells) in ZsGreen^− and ZsGreen^+ lung macrophages 24 h post-i.v. injection of B16ZsGreen in indicated groups of mice by flow cytometry. Statistical differences were determined by Student's unpaired t test.

(C) Schematic overview of metabolomics experiment. WT or *Rptr^{f/f}/LysM^{Cre}* BMDMs were co-cultured with B16ZsGreen at a 5:1 ratio for 24 h followed by FACS of ZsGreen^−, ZsGreen^+, and NT BMDMs. Cells were rested for 1 h, and media were substituted with media containing isotopically labeled glucose (^{13}C) for 2 h,[20] upon which cells were fixed and metabolites were extracted for liquid chromatography/mass spectrometry (LC/MS) analysis.

(D) Normalized fractional contribution of incorporation of ^{13}C-glucose in selected TCA cycle metabolites in FACS ZsGreen$^-$, ZsGreen$^+$, and NT WT or mTORC1-deficient *Rptr$^{f/f}$/ LysM^{Cre}* BMDMs.

(E) Quantification of ATP production in ZsGreen$^-$ or ZsGreen$^+$ macrophages isolated from lungs of indicated groups of mice.

(F) Fold increase of VCAM1, CD38, and CD63 expression on ZsGreen$^+$ over ZsGreen$^-$ lung macrophages in indicated groups of mice. N = 3–5 per group.

(G) Quantification of CD45$^-$ ZsGreen$^+$ tumor cells of total live cells in lungs 24 h post-i.v. injection of B16ZsGreen indicative of metastatic seeding by flow cytometry (n = 19–20 mice/group; pooled data from 5 independent experiments).

All data are representative of at least two independent experiments; **p < 0.01, *p < 0.05 as determined by unpaired Student's t test (B, D, and F), two-way ANOVA and Sidak's multiple comparison test (E), and Mann-Whitney U test (G).

See also Figure S6.

KEY RESOURCES TABLE

REAGENT or RESOURCE	SOURCE	IDENTIFIER
Antibodies		
anti-mouse CD11b - BV605 (clone M1/70)	Biolegend	Cat# 101237; RRID:AB_11126744
anti-mouse CD11c - BV510 (clone N418)	Biolegend	Cat# 117337; RRID:AB_2562010
anti-mouse CD11c - PerCp-Cy5.5 (clone N418)	Biolegend	Cat# 117328; RRID:AB_2129641
anti-mouse CD19 - BV785 (clone 6D5)	Biolegend	Cat# 115543; RRID:AB_11218994
anti-mouse CD24 - PECy7 (clone M1/69)	Biolegend	Cat# 101822; RRID:AB_756048
anti-mouse CD38 - BV711 (clone 90/CD38)	BD BioSciences	Cat# 740697; RRID:AB_2740381
anti-mouse CD38 - PE (clone 14.27)	Biolegend	Cat# 250505; RRID:AB_2563069
anti-mouse CD45 - PerCp-Cy5.5 (clone 30-F11)	Biolegend	Cat# 103132; RRID:AB_893340
anti-mouse CD45 - AF700 (clone 30-F11)	Biolegend	Cat# 103128; RRID:AB_493715
anti-mouse CD45R (B220) - BV785 (clone RA3-6B2)	Biolegend	Cat# 103245, RRID:AB_11218795
anti-mouse CD63 - PE (clone NVG-2)	Biolegend	Cat# 143904; RRID:AB_11204430
anti-mouse CD90.2 - BV785 (clone 30-H12)	Biolegend	Cat# 105331; RRID:AB_2562900
anti-mouse CD103 - APC (clone 2E7)	Biolegend	Cat# 121414; RRID:AB_1227502
anti-mouse CD106 - BV650 (clone 429(MVCAM.A))	BD BioSciences	Cat# 740471; RRID:AB_2740196
anti-mouse CD106 - PE (clone 429 (MVCAM.A))	Biolegend	Cat# 105713; RRID:AB_1134166
anti-mouse Ly6C - BV711 (clone HK1.4)	Biolegend	Cat# 128037; RRID:AB_2562630
anti-mouse Ly6G - BV785 (clone 1A8)	Biolegend	Cat# 127645; RRID:AB_2566317
anti-mouse MHCII (I-A/I-E) - AF700 (clone M5/114.15.2)	Biolegend	Cat# 107622; RRID:AB_493727
anti-mouse MHCII (I-A/I-E) - BV650 (clone M5/114.15.2)	Biolegend	Cat# 107641; RRID:AB_2565975
anti-mouse NK1.1 - BV785 (clone PK136)	Biolegend	Cat# 108749; RRID:AB_2564304
anti-mouse SiglecF - BV785 (clone E50-2440)	BD BioSciences	Cat# 740956; RRID:AB_2740581
Phospho-S6 Ribosomal Protein (ser235/236)XP - PE (clone D57.2 2E)	Cell Signaling Technologies	Cat# 5316S
Phospho-4E-BP1(Thr37/46)- AF647 (clone 236B4)	Cell Signaling Technologies	Cat# 5123S
anti-mouse CD16/32 (clone 2.4G2)	BioXCell	Cat# BE0307
Normal Rat Serum	Thermo Fisher	Cat# 10710C
Biological samples		
Mouse tissue samples (lungs)	UC San Francisco	IACUC: AN184232
Chemicals, peptides, and recombinant proteins		
Dnase I	Millipore Sigma	10104159001
Liberase TM	Roche	5401127001
Rapamycin	Millipore Sigma	553210
Zombie NIR Fixable Viability Dye	Biolegend	423106
Mitotracker Deep Red FM	Thermo Fisher Scientific	M22426
TMRM	Thermo Fisher Scientific	I34361
Low Melting Agarose	Lonza	50080
Recombinant murine M-CSF	Peprotech	315–02

REAGENT or RESOURCE	SOURCE	IDENTIFIER
poly-L-lysine	Sigma-Aldrich	P8920
Critical commercial assays		
Foxp3/Transcription Factor Staining Buffer Kit	BD Biosciences	554655
Seahorse XFe24 Analyzer Extracellular Flux Assay Kit	Agilent Technologies	102340–100
Seahorse XFe96 Analyzer Extracellular Flux Assay Kit	Agilent Technologies	102416–100
Seahorse XF Cell Mito Stress Test Kit	Agilent Technologies	103015-100
UltraComp eBeads Compensation Beads	Fisher Scientific	01-2222-42
Luminescent ATP Detection Assay Kit	Abcam	ab113849
Deposited data		
All bulk RNAseq data	This paper	GEO: GSE230517
InfinityFlow on lung immune cells	Becht et al.[10]	FlowRepository: FR-FCM-Z68V
Experimental models: Cell lines		
B16F1ZsGreen	This paper	N/A
B16F10	AATCC	CRL-6475
B16ZsGreen	This paper	N/A
LLCZsGreen	This paper	N/A
MEFZsGreen	This paper	N/A
Experimental models: Organisms/strains		
Mouse: C57BL/6J	The Jackson Laboratory	Stock# 000664
Mouse: MacBlue	David Hume, Roslin Institute	MGI: 5587942
Mouse: Raptor F/F	Xin Chen, University of California San Francisco	MGI: 4879103
Mouse: Rictor F/F	Xin Chen, University of California San Francisco	MGI: 5448837
Mouse: LysM-Cre (B6.129P2-Lyz2tm1(cre) Ifo/J)	The Jackson Laboratory	Stock# 004781
Mouse: β-actin-Cre (B6.FVB-Tmem163Tg(ACTB-cre)2Mrt/EmsJ)	The Jackson Laboratory	Stock# 033984
Mouse: Ai6 (B6.Cg-Gt(ROSA) 26Sortm6(CAG-ZsGreen1)Hze/J)	The Jackson Laboratory	Stock# 007906
Software and algorithms		
Imaris	Bitplane	https://imaris.exinst.com/
ImageJ	NIH	https://imagej.nih.gov/ij/
FlowJo	Becton Dickinson	https://flowjo.com/
R: The Project for Statistical Computing	N/A	http://r-project.org